metals

MDPI

Article

Synthesis and Characterization of Hollow Glass Sphere Containing Aluminum Syntactic Foam by Spark Plasma Sintering and Hot Pressing

Yong Guk Son [1,2], Young Cheol Lee [1], Sung Su Jung [1], Han Sang Kwon [3], Wookjin Lee [1,*] and Yongho Park [2,*]

1 Korea Institute of Industrial Technology (KITECH), 42-7 Baegyang-daero 804 beon-gil, Busan 46938, Korea; a489756@kitech.re.kr (Y.G.S.); yclee87@kitech.re.kr (Y.C.L.); jungss@kitech.re.kr (S.S.J.)
2 Department of Materials Science and Engineering, Pusan National University, 2 Busandaehak-ro 63 beon-gil, Busan 46241, Korea
3 Department of Materials System Engineering, Pukyong National University, 365 Sinseon-ro Nam-gu 48547, Busan 608737, Korea; Kwon13@pknu.ac.kr
* Correspondence: wkjinlee@kitech.re.kr (W.L.); yhpark@pusan.ac.kr (Y.P.); Tel.: +82-05-367-9409 (W.L.); +82-51-510-3967 (Y.P.)

Received: 4 November 2019; Accepted: 25 November 2019; Published: 27 November 2019

Abstract: The effect of sintering process on the microstructure and the mechanical properties of aluminum syntactic foam were investigated in this study. Two different sintering processes of spark plasma sintering and hot pressing were used. Glass hollow spheres with a size of 50–80 μm was used to fabricate the foams having various volume fractions of the spheres in the range of 10–30%. Microstructural analysis revealed that the glass hollow spheres were uniformly distributed in the aluminum matrix, both in the spark plasma sintered and hot pressed ones. As the volume fraction of the spheres increased from 10 to 30%, the density, micro-hardness and compressive strength of the foams were decreased. In comparison to the foams fabricated by hot pressing method, the spark plasma sintered foams had slightly lower density and mechanical strength. In nanoindentation study, it was found that the aluminum matrix in the foam prepared by the spark plasma sintering process had lower strength than foam prepared by the hot pressing process. This is likely because of shorter sintering time used in the spark plasma sintering process than the hot pressing.

Keywords: aluminum syntactic foam; spark plasm sintering; glass hollow sphere; microstructure; mechanical properties

1. Introduction

Metal syntactic foams are novel composite materials that have controlled voids in their microstructure by embedding glass hollow spheres (GHSs) in the metal matrix. Because of their unique microstructures, they have low density, excellent specific mechanical strength and energy absorption behavior compared to the ordinary metallic materials. Among the various types of metal matrix syntactic foams, aluminum syntactic foams (ASFs) are much lighter compared to the iron-based foams and potentially be used as new materials for light-weight structural components in automobile, marine and aerospace industries [1,2].

One of the easiest methods of fabricating the ASFs is infiltration or stir, followed by casting [3–5]. However, the commercial applications of these methods have been often restricted by their intrinsic limitations of casting. For instance, Hashim et al. [6] reported that ASF manufactured by stirring casting has chemical reactions between the GHS and the matrix alloy. Monddal et al. [7] reported that infiltration casting has a limitation of infiltration thickness and thus, only small size syntactic foam

could be prepared through this technique. Karbalaei et al. [8] reported that ASF manufactured by stirring casting has poor wettability and heterogeneous distribution of the GHS. Vogiatzis et al. [9] reported that the infiltration casting has a difficulty of producing metallic foams with a different volume fraction of GHS. They also pointed out that a significant amount of GHS can easily be broken or filled with matrix during the infiltration process. To overcome these problems, some recent studies have devoted to fabricate ASFs though powder metallurgy route [9–12]. As an example, Vogiatzis et al. [12] investigated to macro and micro structural characteristics, compressive strength and deformation mechanisms of syntactic foams produced by powder metallurgy route at hot pressing (HP) sintering.

In powder metallurgy, materials are mostly produced by HP or Pressure-Less Sintering (PLS) to produce full dense composites. In PLS, parameters, such as low heating rate, higher sintering temperature and long holding time help to fabricate fully dense materials. However, longer holding time and high sintering temperature also lead to coarse grains at the final microstructure, resulting in low mechanical properties. The density and mechanical properties of composites are found to be generally higher in HP than in PLS [13]. On the other hand, spark plasma sintering (SPS) process has lower sintering temperature, short sintering time and higher heating rates than PLS or HP [14,15]. By the high energy plasma that is generated during the process between unconsolidated powders, the dense oxide film on the surface of Aluminum (Al) powder can be easily broken during the SPS process. To the best of the author's knowledge, microstructure and properties of the ASFs fabricated by the HP and SPS process has not been reported in the literature, although these processes are advantageous by the shorter processing time and reliable mechanical properties compared to the PLS [14]. This study aims to investigate the microstructure and mechanical properties of the ASF manufactured by HP and SPS process. The sintering behaviors of the ASFs using the HP and the SPS were investigated in terms of sintering temperature and holding time as well as sintering pressure. The compressive strength, hardness and local deformation behaviors of the ASFs were studied for the foams having different volume fractions of the GHSs, and the results were discussed along with their microstructures.

2. Experimental Procedure

Commercial grade pure Al powder (purity = 99.7%, average particle size = 5 μm) was used as a raw powder for the matrix. Soda lime borosilicate GHS with an average particle size of 50–80μm (24Si-0.2Na-0.1K-16Ca-0.7Mg-0.1 Fe-2.6B-41.4O wt.%, S38HS, 3M^{TM}, United State) was selected for the reinforcing material. The size ratio of the powders between the Al and the GHS were carefully selected to avoid GHS agglomeration by surrounding the GHS with small Al powder. The powders were mixed with volume ratios of 90:10, 80:20 and 70:30 by mechanical mixing. Figure 1 schematically shows the mixing method of the Al and GHS powders. To prepare green bodies, the powders were made in a slurry form by mixing 3 mL of heptane and 6 mL of alcohol for temporarily binding 4.92 g, 4.83 g and 4.71 g of Al and 0.07 g, 0.16 g and 0.28 g of GHS powders. The slurry was then pressed by 30 MPa in a steel mold to fabricate the green bodies. Then the green body was dried in an oven (80 °C for 3 hours) to vaporize the alcohol. Sintering was done in a graphite mold, in both the HP and the SPS processes (SPS-321LX, Fuji Electronic Industrial Co. Ltd., Tsurugashima, Japan). The sintering pressure was fixed to 30 MPa for all the experiments, because preliminary tests with various compact pressure to prepare the green body showed that the breakage of the GHS occurred at a pressure higher than 30 MPa. Table 1 summarizes the sintering behaviors of foams according to various sintering temperatures and holding times. The main results can be summarized as follows:

(1) Among the temperature range tested, the sintering temperature of 600 °C was the best for the HP process. When the sintering temperature is lowered to 550 °C, there was not enough bonding between the Al powders during the sintering process. Significant damage of the GHS occurred when higher sintering temperature of 650 °C was used.

(2) In the case of the SPS process, both the sintering temperature and the holding time could be significantly reduced compared to the HP process. The sintering temperature of 550 °C with

holding time of 15min was the best for the SPS process. Increasing the holding time to 30 min when keeping sintering temperature, the same significantly increased the final density of the foams, due to the softening of the GHS. Similar behavior was observed when the sintering temperature was raised to 600 °C.

Therefore, for the HP process, the processing parameters for producing the samples were chosen by the holding time of 1hour and the sintering temperature of 600 °C. For the SPS process, the holding time of 15 min and the sintering temperature of 550 °C were chosen. The relative density of sintered specimens was measured by the Archimedes method. Microstructures of the specimens were investigated by Optical Microscopy (OM, Leica DM 2700M RL/TL, Leica, Wetzlar, Germany) and Scanning Electron Microscope (SEM, S-4800, Hitachi, Tokyo, Japan). The mechanical properties of the sintered specimens were evaluated by uniaxial compressive tests (Keitnley US/2400 R&B Korea, Korea). The compressive tests were carried out three times for each of the ASF specimens containing 10, 20 and 30 vol.% fabricated by HP and SPS sintering process at a strain of 10^{-3} s^{-1} on a rectangular specimen of a volume of 3 × 3 × 6 mm. The localized mechanical properties of the specimens were also investigated by the micro hardness tests (HMV-2T, Shimadzu, Kyoto, Japan) and nano-indentation (Anton paar NHT2, Anton paar, Auckland, New Zealand).

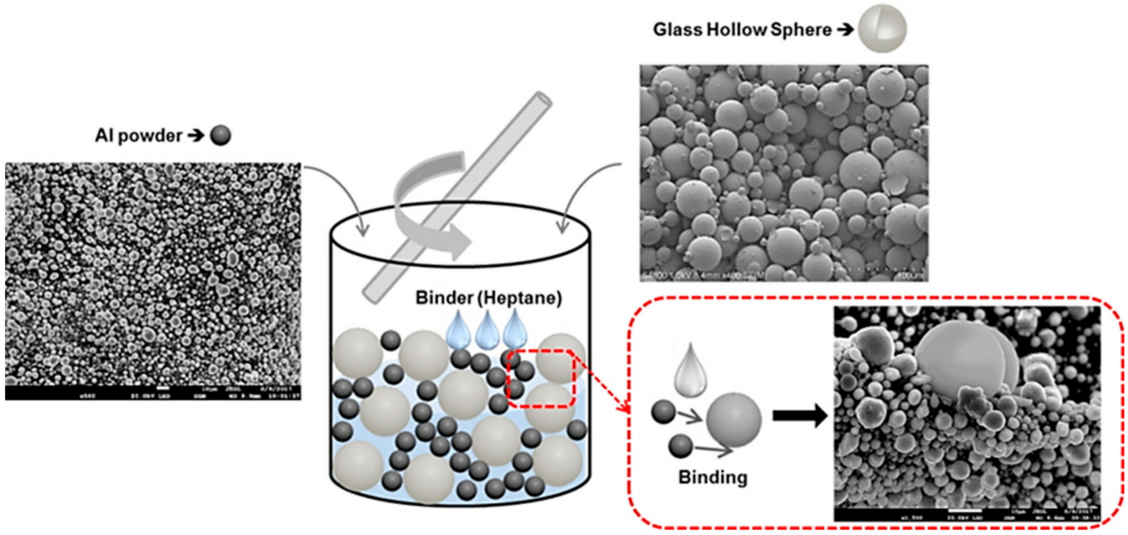

Figure 1. Schematics of the mixing method of Al and glass hollow spheres (GHS) raw powders.

Table 1. Sintering behavior of the aluminum syntactic foams (ASFs) in terms of different sintering time and temperature. HP, hot pressing; SPS, spark plasma sintering.

Sample Type (Vol.%)	Sintering Method	Sintering Temp (°C)	Holding Time	Sintering Behavior
GHS 30%	HP	550	1 h	Poor bonding
		600		Good
		650		GHS Softening or Broken
	SPS	550	15 min	Good
		550	30 min	GHS Softening or Broken
		600	15 min	GHS Softening or Broken

3. Results and Discussions

Figure 2 shows the evolutions of the relative densities of the ASFs with increasing volumes of GHSs. The densities were measured from local parts from the bottom, middle, and top of each sample, and it was found that the density was uniform throughout for every specimen tested. The density

decreased with increasing the GHS volume fraction. The theoretical density, D_{comp}, of the ASF can be predicted using the following equations.

$$D_{comp} = (D_{GHS} \times V_{GHS}) + (D_{Al} \times V_{Al}), \quad (1)$$

where D_{GHS} and D_{Al} denote the true densities of the GHS and the Al, respectively. V_{GHS} and V_{Al} are volume fractions of the GHS and Al, respectively. Values for the true densities of the GHS and the Al are taken as listed in Table 2 for the calculations. The theoretical density of ASF calculated by Equation (1) is shown in Figure 2 for comparison. Specimens without GHSs (100% Al) have a relative density of 95% and 91%, compared to the theoretical density, for the HP and SPS, respectively. In these cases, the difference between the theoretical and the relative densities of the specimens can be explained by formations of unintended micro porosity, due to insufficient bonding between Al particles during the sintering process. As the volume fraction of the GHS increased, the relative density decreased sharply both in the HPed and SPSed specimens. The ASFs containing 10 vol.% GHS have a relative density close to 100% of the theoretical density for specimens prepared by the HP, and 97% for the specimens prepared by the SPS. When the volume fraction of the GHS increased to 20 and 30%, the relative density becomes slightly higher than the theoretical densities. This increase can be attributed to the pore volume reductions as Al powder filled in the damaged GHSs during the sintering processes [16,17]. It was found that the ASF fabricated by the HP process has relative densities generally higher than the ASF fabricated by the SPS process. The reason why the ASF fabricated by the HP process is denser than the ASF fabricated by the SPS process is thought to be from denser Al matrix than in the SPS process, since there was no microstructural evidence that more broken GHS exists in the foams fabricated by the HP process than in the samples fabricated by the SPS.

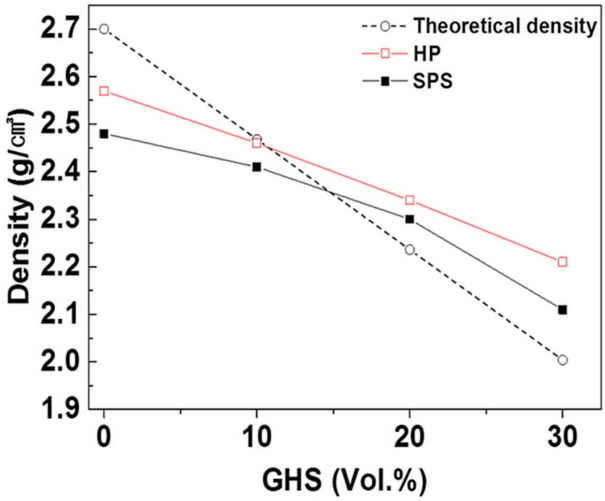

Figure 2. Relative density according to the increasing of GHSs volumes content of the within ASF prepared at 600 °C for 1 h in HP process and 15 min at 550 °C in the SPS process.

Table 2. Physical properties of the glass hollow sphere and aluminum used for the study.

Powder Type	True Density (g/cm^3)	Vol.% Glass	Vol.% Gas
GHS	0.38	15	85
Al	2.7	-	-

Figure 3 shows the microstructures of the sintered specimen fabricated by the HP and SPS process. In the both samples fabricated by the HP and the SPS process, GHSs were homogenously distributed inside the ASFs. In the HPed specimen, most of the GHS remains in a circular shape after the sintering process. However, in the SPSed specimen, most of the GHS particles became elliptical shapes during

the process. In order to compare statistically the shape of the GHS in the microstructures from the syntactic foam fabricated by the HP and the SPS, the ratio between the diameters of in the vertical and horizontal directions with respect to the pressing direction was analyzed by an image analysis software (I-solution DT, IMG Technology, Burnaby, Canada). The ratios of the largest 9 GHSs from each of 20 individual OM images with a magnification of 200× were characterized for the specimens having 30% GHS. Thus, in total, the ratios of 360 individual GHSs (i.e., 180 GHSs of the specimen fabricated by the HP and another 180 GHSs of the specimen fabricated by the SPS) were analyzed. The shape of the GHS was characterized as an elliptical when the aspect ratio was higher than 1.1, i.e., diameter in the direction horizontal to the pressing direction was larger than 110% of diameter in the vertical direction. The results indicated that the GHSs of the specimen produced by the HP process were 93% circular and 7% elliptical. The GHSs of the sample produced by the SPS process was 50% circular and 50% elliptical. Figure 4 shows closer looks of the GHSs after the sintering processes. In the figure, arrows A indicates the broken and perforated GHS by compaction pressures applied during the sintering process. Arrows B indicates the broken GHS partially filled with the Al powders. Arrows C indicate the deformation of GHS, due to broken and softening of GHS shells by increased local sintering temperature around the GHS. As shown in Figure 4a, the ASF fabricated by the HP process is characterized by fractured GHSs, due to the sintering pressure as indicated by the arrows A and B. The ASF fabricated by the SPS is characterized by the softened GHS shells as indicated by arrows C in Figure 3b. As indicated by Shi-XueSong et al. [18], the sintering temperature can be locally further increased around the ceramic particles in the SPS process. Therefore, the shape change of the hollow body and the GHS shell thickness change occurred due to the local temperature increase around the shell of GHS.

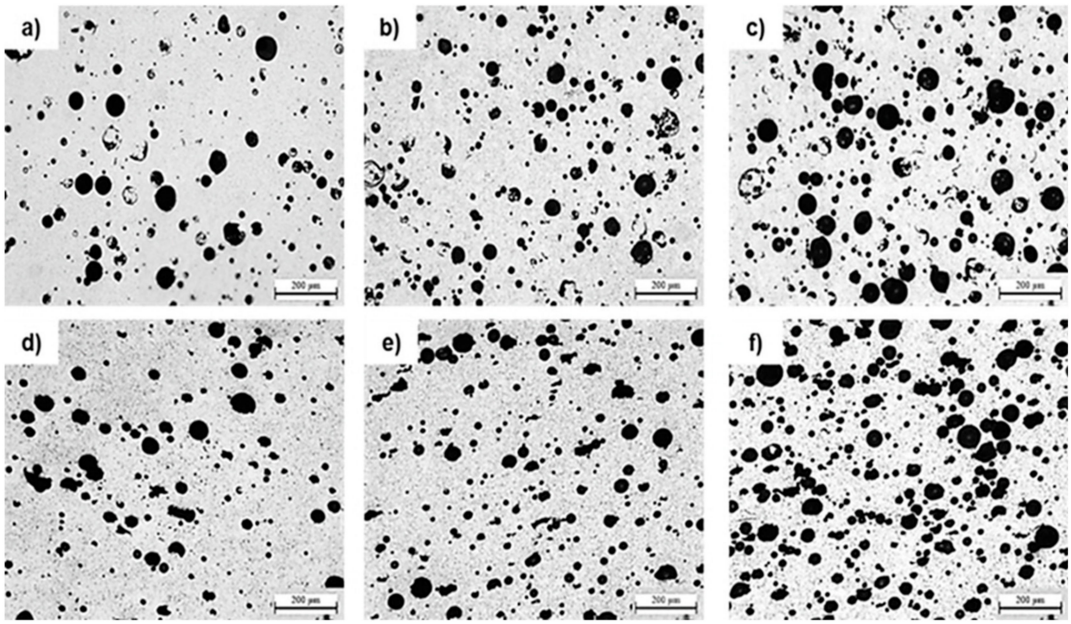

Figure 3. OM images of ASF containing (**a**) 10, (**b**) 20 and (**c**) 30 vol.% GHSs fabricated by HP process at 600 °C and 1 h and (**d**) 10, (**e**) 20 and (**f**) 30 vol.% GHSs fabricated by SPS process at 550 °C and 15 min.

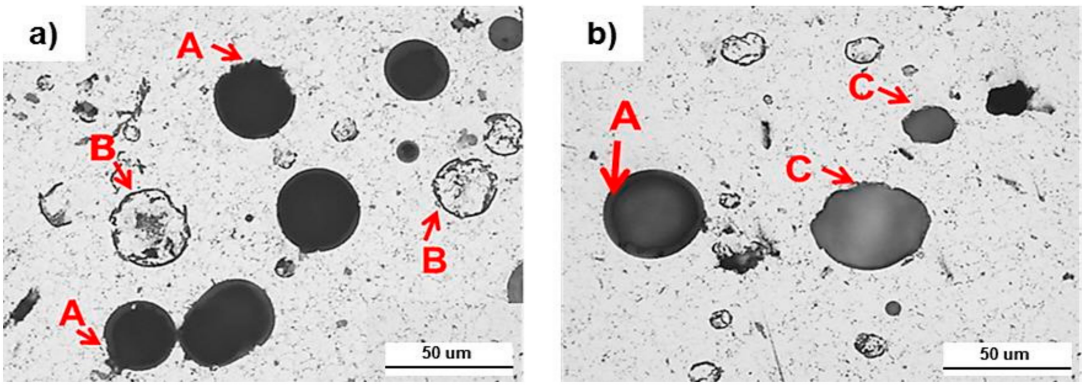

Figure 4. Closer looks of GHS inside ASF containing 30 vol.% GHSs after the sintering process for (**a**) the fabricated by HP process; (**b**) the fabricated by SPS process.

Figure 5 shows energy dispersive X-ray (EDX) line profiles of the chemical elements near the Al/GHS interface. As shown in Figure 5a, there is no pronounced diffusion of any element between the matrix and the GHS shell fabricated by the HP process. This result implied that simple mechanical bonding is occurred without any chemical process between the Al and the GHS during the HP process, by confining the GHS within the shrunk Al matrix during the cooling down to room temperature after the sintering process. Contrastingly, it is clearly shown in Figure 5b that Al has diffused into the GHS shell in the SPS process. This is interesting because the sintering temperature of 550 °C in the SPS is lower than the sintering temperature of 600 °C in the HP process. In general, the diffusion bonding is known to increase the interfacial strength of the reaction layer, due to the chemical reaction between the metal powder and the ceramic powder [19,20]. Therefore, it is expected that the interface strength will be stronger than the foams fabricated by the HP process, due to the diffusion bonding into the GHS shell of the foam fabricated by the SPS process.

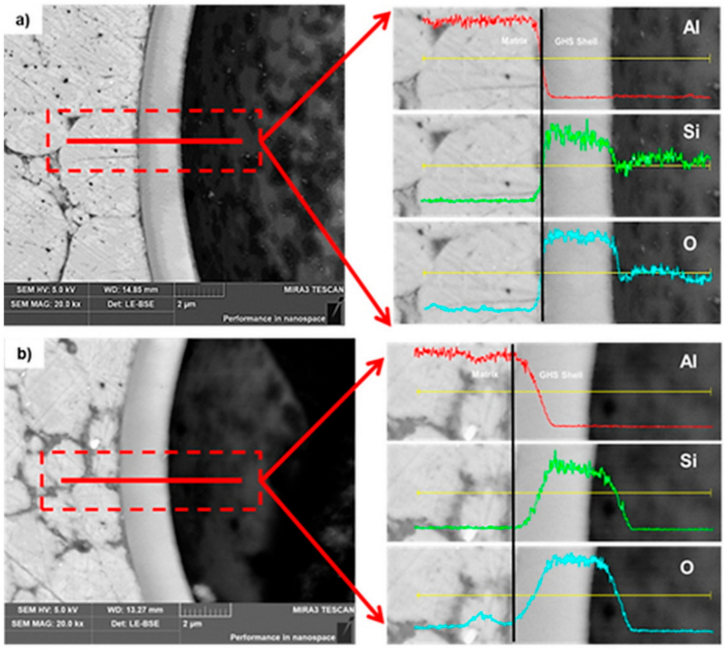

Figure 5. EDS line profile analysis result for Al/GHS interface with the SEM image of ASF containing 30 vol. % GHSs for (**a**) the fabricated by HP process; (**b**) the fabricated by SPS process.

Figure 6 shows the micro hardness of the sintered specimens fabricated by a different sintering process at various GHS fractions. The hardness of the ASF fabricated by the HP was higher than that of the ASF fabricated by SPS. This result is expected to increase the hardness by increasing the sintered

density of the Al matrix of ASF fabricated by HP process. The hardness decreased sharply as the volume fraction of the GHS increased. This is perhaps from increasing the porosity of the foams as the GHS content increases.

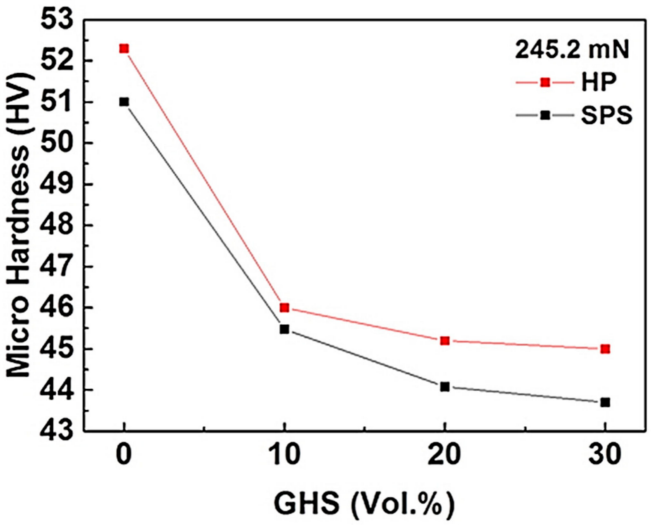

Figure 6. Micro hardness of the sintered specimens fabricated by a different sintering process at various GHS fractions.

In general, compressive stress-strain curves of the syntactic foams could be divided into three stages [16,21]. The initial stage is the pure elastic stage, which results in the closure of micro-pores in the matrix. The second stage is the plateau regions, where GHS breaking or collapse occurs, and shear failure begins between matrix and GHS at the same time. At the final stage, all the GHS are broken, and the densification of the Al matrix occurs when the load is uniform in the matrix. Figure 7 shows the compressive stress-strain curves for the specimens having different GHS volume fractions. To verify the reproducibility and repeatability of this study, three times repeated compressive tests were performed on each type of specimen. The three individual test results reproduced each other very well, and there was no meaningful difference in the compressive stress-strain curves. As the GHS volume fraction increases, the graph appears similar to the general compressive behavior of syntactic foam. As shown in Figure 7a, foams fabricated by HP process showed that the plateau region increased as the content of GHS increased. A similar trend was also observed in the foams fabricated by the SPS. When there was no GHS (pure Al), the HPed specimen showed much higher maximum compressive strain than that from the SPS. With GHS content of 10%, the foam fabricated by the HP process showed significantly lower maximum compressive strain compared to the case of the specimen having no GHS. The maximum compressive strain of the foams then increased with increasing the GHS contents, and when the GHS content was 30%, the maximum compressive strain of the foam was higher than the HPed Al without GHS. In contrast, the foams fabricated by the SPS process showed a sharp decrease in strength and much higher maximum compressive strain when 10% of GHS was introduced, compared to the case of the specimen having no GHS. In this case, the maximum compressive strains were slightly decreased with increasing the GHS contents, as shown in Figure 7b. For the specimens having the highest GHS contents of 30%, the plateau region was more clearly observed in the SPS than in the HP. This is likely because the foams fabricated by the SPS process has superior interfacial bonding between the GHS and the Al compared to those fabricated by the HP process, due to the diffusional process on the interface, as previously shown in Figure 5. The better the interfacial strength is, the better the load transfer between the matrix and the GHS is, which can lead to homogeneous stress distribution and overall deformation during the compression. Figure 8 shows the specimens deformed structure after compressive test on specimens with a different GHS volume fraction. The compressive behaviors of all specimens tested were characterized by the brittle fracture with sharp stress drop occurring

with the collapse of the structure or with shear crack formation. As can be seen in Figure 8, the pure Al specimens produced by the HP and the SPS were collapsed with formations of small and many cracks inside, due to the stress localization, which is clearly indicated by the so-called 'barreling' effect, i.e., lateral expansion on the middle of the specimens during the collapse, as shown in Figure 8. The specimens containing 10 and 20 vol.% GHS showed similar fracture behaviors to the pure Al specimens. When the GHS contents were increased to 30 vol.%, the fracture of the specimens occurred by the shear crack formations.

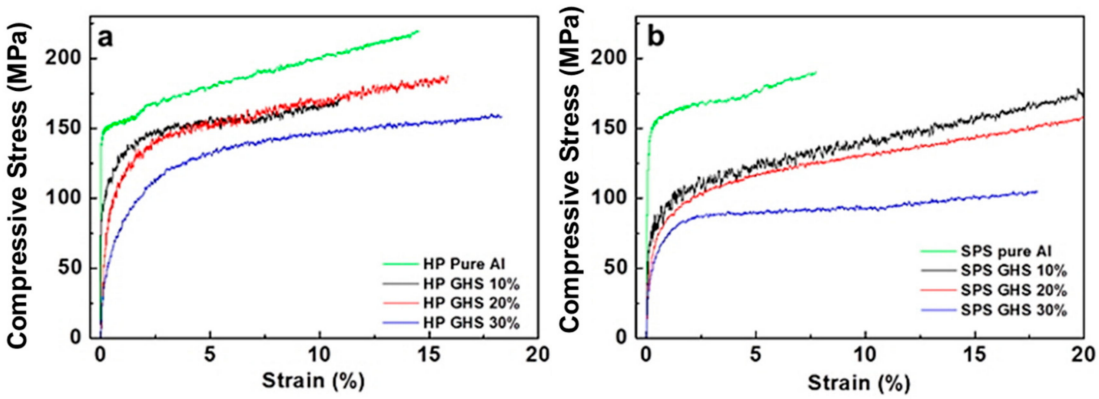

Figure 7. Representative compressive stress-strain curves of specimens with a different GHS powder volume fraction for (**a**) the fabricated by HP process; (**b**) fabricated by SPS process.

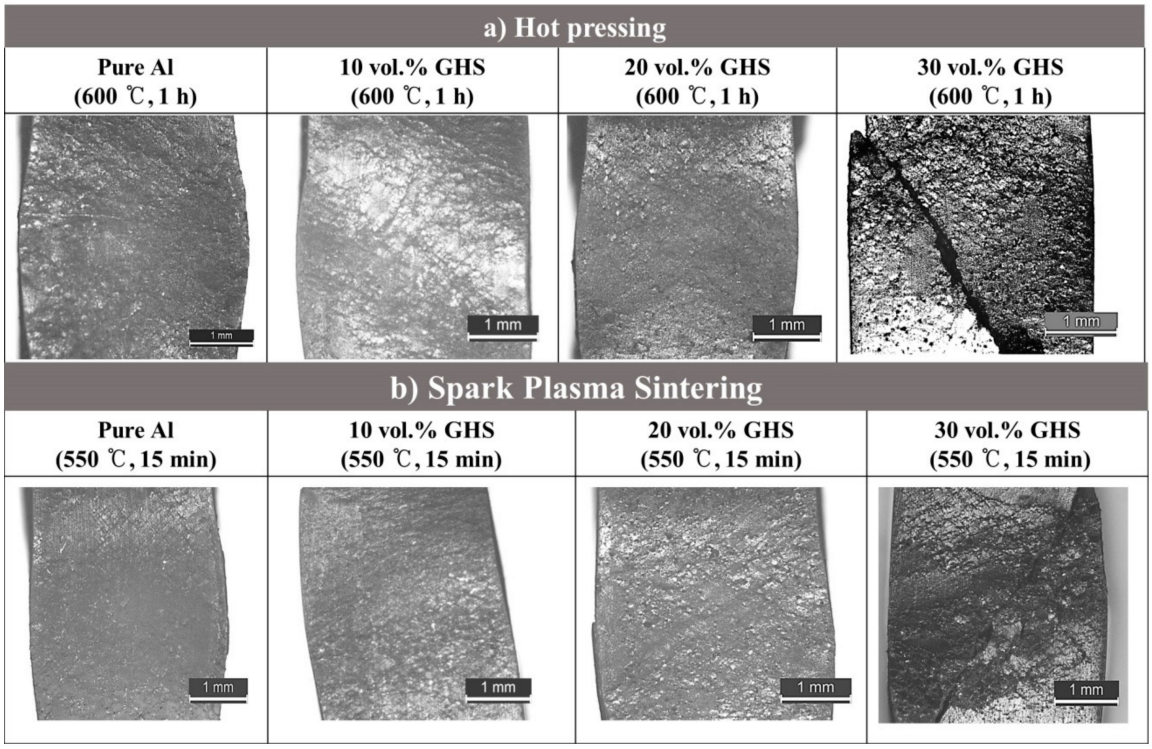

Figure 8. Specimens deformed structure after compressive test of specimens with a different GHS powder volume fraction for (**a**) the fabricated by HP process; (**b**) fabricated by SPS process.

Figure 9a shows the compressive yield strength and specific strength of ASF fabricated by a different sintering process. The compressive yield strength tends to decrease as the GHS content increase, both in the HP and the SPS processes. This behavior can be easily understood by considering that the GHS have a relatively low compressive strength than the sintered Al. The ASF made by the SPS tends to have a lower compressive yield strength than the ASF made by the HP process.

The theoretical Young's modulus in syntactic foams had been investigated recently by Maurizio et al. [22], who proposed an analytical solution based on the rule of the mixture as follows:

$$E_{asf} = E_g(1 + f_E(E_m, \upsilon_m, E_g, \upsilon_g, \eta)\mathrm{V}), \tag{2}$$

where E_{asf} is the theoretical Young's modulus of syntactic foam, E_m and E_g are the young's moduli of the Al and the GHS, respectively. υ_m and υ_g are the Poisson's ratios of the Al and the GHS. η denote the ratio of the inner and outer radii of the glass wall in the GHS. Table 3 lists the physical parameters for the Al and GHS used for calculating the theoretical Young's modulus of the ASF. f_E is a function given by:

$$f_E = \frac{1}{E_m}(h_k(1 - 2\upsilon_g)^2 + \frac{4}{3}h_\mu(1 + \upsilon_g)^2), \tag{3}$$

where h_k and h_μ are parameters related to the shear and bulk moduli of the Al and GHS [22]. The theoretical moduli of the foams calculated by Equations (2) and (3) are plotted along with the experimental measurements in Figure 9b. In the experiments, the Young's moduli decreased both in the HP and SPS processed specimens as the GHS content increases. It is clearly observed that the foams fabricated by both the HP and SPS exhibit slightly lower elastic coefficients than the theoretical ones. One possible reason for this low moduli is the presence of fractured GHS fragments in the ASFs, which can cause insufficient bonding between the Al particles and reduce the modulus of elasticity [12].

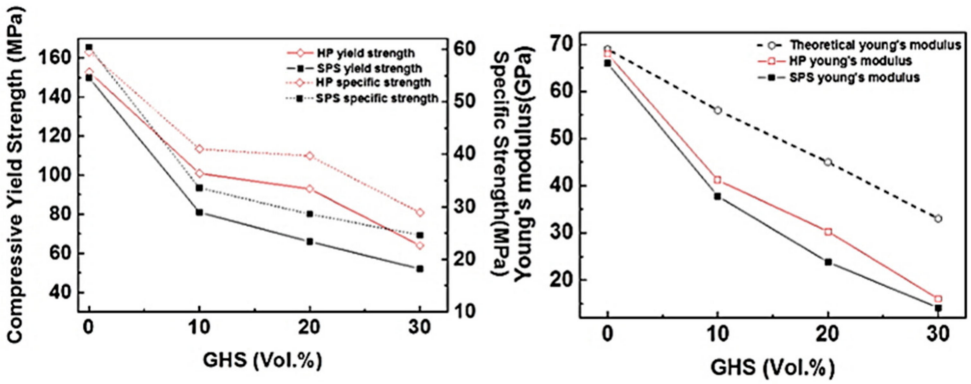

Figure 9. Compressive yield strength, specific strength and young's modulus of different GHS powder vol.% for (**a**) the fabricated by HP process at 600 °C and 1 h; (**b**) the fabricated by SPS process at 550 °C and 15 min.

Table 3. Physical parameters of the Al and GHS.

Material	Elastic Modulus (GPa)	Poisson's Ratio	η	Shear Modulus (GPa)	Bulk Modulus (k) (GPa)
Matrix	68	0.36	-	25	62
GHS	37.1	0.17	0.952	31.2	36.7

Figure 10 shows indentation depths of the Al matrix and the GHS shell of the ASF with 30 vol.% GHS. Figure 10a shows indentation depth for the matrix fabricated by a different sintering process. The ASF sintered by the HP process has a lower indentation depth than the ASF sintered by the SPS process. This result is because the Al matrix of ASF fabricated by HP process is stronger than that Al matrix of ASF fabricated by SPS process. Figure 10b shows the difference in indentation depth of the GHS shell inside the ASF fabricated by the HP and SPS processes. The ASF fabricated by the two sintering processed has the same penetration depth curve and the indentation depth. These results indicate the strength of the glass wall in the GHS is retained during the SPS process even though there are locally high temperature and diffusional process. This indicates that the ASF fabricated by the

SPS process is due to the strength of the Al matrix with lower mechanical properties than the ASF fabricated by the HP process.

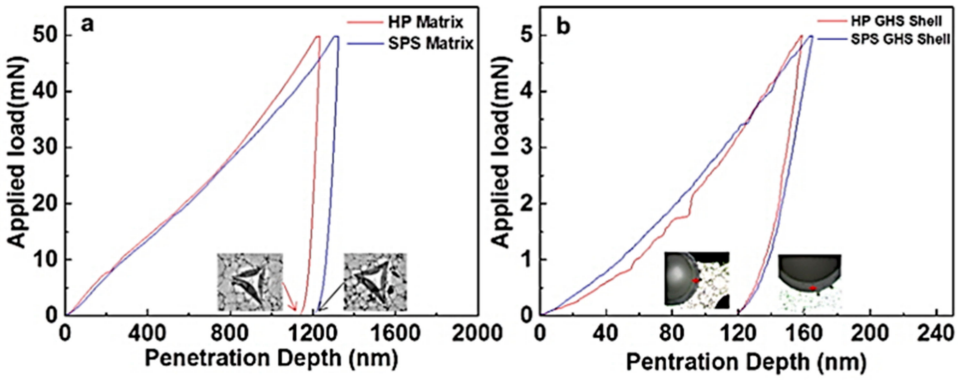

Figure 10. Penetration depth curve of ASF containing 30 vol.% GHSs fabricated by a different sintering process for (**a**) matrix strength; (**b**) GHS strength.

In this study, no more than 30% of GHS by volume was added to maintain the overall compressive strength of the syntactic foam to be suitable for use with GHS as a structural material. The higher volume fraction of GHS in the ASF may further reduce the density of the foam, but significantly reduce the strength. For instance, in the previous study by Vogiztzis et al. [12], ASFs containing 20, 30 and 40 vol.% hollow sphere were produced using powder metallurgy. Ceramic cenospheres having better high-temperature resistance than the GHS was used for their study. The final densities of 0.83, 0.96 and 0.97 g/cm^3 and the compressive strengths of 27.9, 35.2 and 25.8 MPa were reported for the foams having 20, 30 and 40 vol.% cenospheres, respectively. It can be seen that the density was lower than the foams produced in this study, but the compressive strength was much lower than the values observed in this study. Tao and Zhao [3] fabricated an ASF containing hollow spheres up to 63 vol.% by infiltration process, but they should use high performance ceramic hollow spheres having high melting point to fabricate the foams by casting and infiltration. Luong et al. [23] also tried to fabricate an ASF containing 60 vol.% SiC hollow sphere by infiltration followed by the casting process. The final density of the foam in their study was 1.8 g/cm^3, that is only slightly lower density compare to the foams made in this study with 30 vol.% GHS.

It is shown that the microstructure and mechanical properties of foams can be greatly modified by the sintering process. In the case of foams fabricated by the SPS process, the shape of the GHS inside the foam was changed as the local temperature around the GHS became close to the softening temperature. In addition, the interface strength, due to diffusion bonding into the softened GHS shell was further enhanced. The nanoindentation study showed that the strength of the matrix was higher in the ASF fabricated by HP process than the ASF fabricated by SPS process. This is likely because of higher densification in the HP process than the SPS, due to the longer sintering time. The GHS in the ASF fabricated by SPS process had ellipsoidal shapes, due to softening, but the mechanical strength of the glass wall was retained, i.e., the mechanical strength of the glass wall in the SPSed specimen was almost the same to that of the HPed one. By two different pressurized sintering processes used in this study, e.g., HP and SPS, it was able to obtain sound foams having up to 30% of GHS at around 550–600 °C. These processing temperatures are much lower than the temperature required in the conventional casting fabrication process of the ASFs, which is around 730–850 °C [24,25]. The low processing temperature used in this study enabled to have the controllable shape of the pores in the ASF, as most of the GHS in the foams remained unbroken during the process. This controlled microstructure seems to make the HP and SPS processes attractive to fabricate structural materials with high reliability. The short processing times of 0.5 to 1 h required in the pressurized sintering processes are perhaps another advantage to obtain better productivity of the material.

4. Conclusions

1. By pressurized sintering processes of hot pressing and spark plasma sintering, aluminum syntactic foams with volume fractions of glass hollow microspheres up to 30% could be successfully fabricated. The pressurized sintering processes were characterized by short sintering time and low sintering temperatures. In the case of hot pressing, fully dense foams could be fabricated at a sintering temperature of 600 °C with a sintering time of 1 h. Spark plasma sintering process enabled fabricating near fully dense foams with even lower sintering temperature of 550 °C and very short sintering time of 15 min.
2. In the microstructure, some fractured microspheres were observed during the process in both the hot pressing and spark plasma sintering. The fracture of the microspheres seems to be occurred by the pressure applied during the sintering processes. Unbroken microspheres in the hot pressed foam remained in spherical shape, while those in the spark plasma sintered foam became ellipsoidal, due to softening of the glass shell. The deformation of the microsphere in the spark plasma sintered foam is probably, due to local temperature increments around the glass hollow spheres during the sintering process by the plasma.
3. In the case of hot pressing, there was almost no chemical interaction on interfaces between the aluminum matrix and the microspheres. Whereas, the pronounced diffusional process occurred at the interfaces in the foams fabricated by the spark plasma sintering even though lower sintering temperature than the hot pressing was used. This result indicates that the aluminum syntactic foams fabricated by spark plasma sintering has a stronger interfacial strength of the reaction layer than the aluminum syntactic foams fabricated by hot pressing process, due to diffusion bonding.
4. The aluminum syntactic foams fabricated by spark plasma sintering process had slightly lower hardness and compressive strength than the foams fabricated by hot pressing. Nanoindentation results showed that the main reason for the lower strength of the spark plasma sintered foam is lower strength of aluminum matrix in the spark plasma sintered foam than in the hot pressed one. On the other hand, the maximum compressive strain was higher in the spark plasma sintered foam than those fabricated by hot pressing process, due to the strong chemical bonding at the interfaces between the microsphere and the aluminum matrix.

Author Contributions: Planning and designing of experiments were done by W.L. and Y.C.L., and experiments were done by Y.G.S. and S.S.J. with supervision of H.S.K. Writing was done by Y.G.S. and reviewed by W.L. and Y.P.; Writing-review and editing, Y.P., Y.C.L. and W.L.

Funding: This research was funded by the Ministry of SMEs and Startups (MSS), grant number PIZ19550.

Acknowledgments: This work was supported by a Korea Evaluation Institute of Industrial Technology(KEIT) grant funded by the Korea government (MOTIE) (No. PIZ19550, Development of Core Material for ISO Container Type Small Scale LNG Plant).

Conflicts of Interest: The authors declare no conflict of interest. The funders had no role in the design of the study; in the collection, analyses, or interpretation of data; in the writing of the manuscript, or in the decision to publish the results.

References

1. Gupta, N.; Rohatgi, P.K. *Metal. Matrix Syntactic Foams: Processing, Microstructure, Properties and Applications*; DEStech Publications, Inc.: Lancaster, PA, USA, 2015.
2. Singh, N.P.; Purgert, R.M.; Sobczak, J. Aluminum Syntactic Foams Alfa for Automotive Applications. *J. KONES Intern. Combust. Engines* **2003**, *10*, 3–4.
3. Tao, X.F.; Zhao, Y.Y. Compressive behavior of Al matrix syntactic foams toughened with Al particles. *Scr. Mater.* **2009**, *61*, 461–464. [CrossRef]
4. Lin, Y.; Zhang, Q.; Wu, G. Interfacial microstructure and compressive properties of Al-Mg syntactic foam reinforced with glass cenospheres. *J. Alloy. Compd.* **2016**, *655*, 301–308. [CrossRef]

5. Rajan, T.P.D.; Pillai, R.M.; Pai, B.C.; Satyanarayana, K.G.; Rohatgi, P.K. Fabrication and characterisation of Al-7Si-0.35Mg/fly ash metal matrix composites processed by different stir casting routes. *Compos. Sci. Technol.* **2007**, *67*, 3369–3377. [CrossRef]
6. Hashim, J.; Looney, L.; Hashmi, M.S.J. Metal matrix composites: Production by the stir casting method. *J. Mater. Process. Technol.* **1999**, *92*, 1–7. [CrossRef]
7. Mondal, D.P.; Das, S.; Ramakrishnan, N.; Bhasker, K.U. Cenosphere filled aluminum syntactic foam made through stir-casting technique. *Compos. Part. A Appl. Sci. Manuf.* **2009**, *40*, 279–288. [CrossRef]
8. Akbari, M.K.; Mirzaee, O.; Baharvandi, H.R. Fabrication and study on mechanical properties and fracture behavior of nanometric Al_2O_3 particle-reinforced A356 composites focusing on the parameters of vortex method. *Mater. Des.* **2013**, *46*, 199–205. [CrossRef]
9. Vogiatzis, C.A.; Skolianos, S.M. On the sintering mechanisms and microstructure of aluminium-ceramic cenospheres syntactic foams produced by powder metallurgy route. *Compos. Part. A Appl. Sci. Manuf.* **2016**, *82*, 8–19. [CrossRef]
10. Guo, R.Q.; Rohatgi, P.K.; Nath, D. Preparation of aluminium-fly ash particulate composite by powder metallurgy technique. *J. Mater. Sci.* **1997**, *32*, 3971–3974. [CrossRef]
11. Spratt, M.; Newkirk, J.W.; Chandrashekhara, K. Aluminum Matrix Syntactic Foam Fabricated with Additive Manufacturing. *Solid Free Fabr. Symp.* **2017**, 242–248.
12. Vogiatzis, C.A.; Tsouknidas, A.; Kountouras, D.T.; Skolianos, S. Aluminum-ceramic cenospheres syntactic foams produced by powder metallurgy route. *Mater. Des.* **2015**, *85*, 444–454. [CrossRef]
13. Madhan, M.; Prabhakaran, G. Microwave versus conventional sintering: Microstructure and mechanical properties of Al_2O_3-SiC ceramic composites. *Boletín de la Sociedad Española de Cerámica y Vidrio* **2019**, *58*, 14–22. [CrossRef]
14. Kwon, H.; Park, D.H.; Park, Y.; Silvain, J.F.; Kawasaki, A.; Park, Y. Spark plasma sintering behavior of pure aluminum depending on various sintering temperatures. *Met. Mater. Int.* **2010**, *16*, 71–75. [CrossRef]
15. Borrell, A.; Salvador, M.D. Advanced Ceramic Materials Sintered by Microwave Technology. *Sinter. Technol.-Method Appl.* **2018**, 3–24.
16. Cho, Y.J.; Lee, T.S.; Lee, W.; Lee, Y.C.; Park, Y.H. Preparation and Characterization of Iron Matrix Syntactic Foams with Glass Microspheres via Powder Metallurgy. *Met. Mater. Int.* **2019**, *25*, 794–804. [CrossRef]
17. Movahedi, N.; Taherishargh, M.; Belova, I.V.; Murch, G.E.; Fiedler, T. Mechanical and microstructural characterization of an AZ91-activated carbon syntactic foam. *Materials (Basel)* **2018**, *12*, 3. [CrossRef]
18. Song, S.X.; Wang, Z.; Shi, G.P. Heating mechanism of spark plasma sintering. *Ceram. Int.* **2013**, *39*, 1393–1396. [CrossRef]
19. Lemus-Ruiz, J.; Ceja-Cárdenas, L.; Verduzco, J.A.; Flores, O. Joining of tungsten carbide to nickel by direct diffusion bonding and using a Cu-Zn alloy. *J. Mater. Sci.* **2008**, *43*, 6296–6300. [CrossRef]
20. Ratnaparkhit, P.L.; Howe, J.M. Structure and mechanism of bonding at a diffusion-bonded A1/SiC interface. *Acta Metall. meterialia.* **1994**, *42*, 811–823. [CrossRef]
21. Zhao, Y.Y.; Tao, X.F. Behaviour of Metal Matrix Syntactic Foams in Compression. *Mater. Sci. Technol.* **2009**, *4*, 1785–1794.
22. Porfiri, M.; Gupta, N. Effect of volume fraction and wall thickness on the elastic properties of hollow particle filled composites. *Compos. Part. B Eng.* **2009**, *40*, 166–173. [CrossRef]
23. Luong, D.D.; Strbik, O.M.; Hammond, V.H.; Gupta, N.; Cho, K. Development of high performance lightweight aluminum alloy/SiC hollow sphere syntactic foams and compressive characterization at quasi-static and high strain rates. *J. Alloy. Compd.* **2013**, *550*, 412–422. [CrossRef]
24. Zhang, L.P.; Zhao, Y.Y. Mechanical response of Al matrix syntactic foams produced by pressure infiltration casting. *J. Compos. Mater.* **2007**, *41*, 2105–2117. [CrossRef]
25. Lin, Y.; Zhang, Q.; Ma, X.; Wu, G. Mechanical behavior of pure Al and Al-Mg syntactic foam composites containing glass cenospheres. *Compos. Part. A Appl. Sci. Manuf.* **2016**, *87*, 194–202. [CrossRef]